Turbulent Drag Reduction Using Three-Dimensional Structured Surfaces

Yulia Peet, Pierre Sagaut

Université Pierre et Marie Curie - Paris 6, F-75252, Paris Cedex 05, France

Yves Charron

Institut Français du Pétrole - IFP, F-92852, Rueil Malmaison Cedex, France

1   Introduction

Structured surfaces are the surfaces covered with riblets, or wall grooves. They are attractive drag-reducing devices because of their low production cost and easiness of maintenance [1, 2, 3, 4, 5, 6, 7, 8]. They can be successfully installed on wings of an aircraft, hull of a submarine or internal walls of a gas pipeline by adding special plastic films with sub-millimeter scale riblets which are available commercially[7, 9]. An unfortunate disadvantage of riblets is rather low amount of drag reduction which they can offer: the best values have been achieved with infinitely-thin blade riblets giving about 10% reduction for an optimized configuration [8]; while more realistic cross-sections for industrial use, such as triangular, V-groove or scalloped, usually account for 4–8% drag reduction [1, 2, 3, 4, 5, 6, 7, 8]. An easy modification to the riblet method, retaining its structural simplicity but improving its drag reduction performance, would be more than welcome!

One of the new methods proposed in literature devoted to turbulent skin-friction drag reduction is high-frequency spanwise wall oscillations [10, 11, 12, 13, 14, 15]. It is argued that oscillatory motion of the wall makes longitudinal boundary layer vortices move in a sinuous form, which reduces their strength and, consequently, their ability to produce turbulence through near-wall burst events [16], resulting in a lower turbulent skin-friction drag. In practical applications, it is usually not possible to provide sustainable oscillations of the surface. However, if one can mimic such an oscillatory motion with the help of some passive devices, that should have more or less similar effect. In was recently proposed to use riblets to guide the flow into oscillatory motion by changing the shape of riblets from conventional straight rods into sinusoidal rods [17]. By combining these two drag reduction mechanisms (riblets and oscillatory flow motion), it is hoped that the benefits of the two methods will also be combined.

In this paper, we document Large Eddy Simulation (LES) study of turbulent flow in a channel, one wall of which is covered with riblets of triangular cross-section, and the other wall is flat. Computations of three geometries are performed: conventional straight riblets (with the results compared to DNS data of Choi et al. [6]) and two cases of sinusoidal riblets with different wave-

lengthes of riblet oscillations. It is found that the wavelength of riblet oscillations equal to $3.22\,\delta$ results in a smaller drag reduction than the straight riblet case. However, if the wavelength is increased to $6\,\delta$, drag reduction achieved with the sinusoidal riblets is about 50% larger than that with the straight riblets, demonstrating clear benefits of the former method. Strong dependence of drag reduction properties on the oscillation period was also reported for the case of spanwise-oscillating wall [10, 18], phenomenon not yet understood.

2   Numerical Method and Validation

Computational code used to perform LES of the riblet geometry is Code_Saturne [19] developed at Électricité de France (EDF). The code is fully conservative, second-order, unstructured finite volume solver with collocated arrangement of variables. It solves incompressible Navier-Stokes equations using fractional step method, where the pressure correction step leads to Poisson equation for pressure. The code has been used for calculation of many industrial problems in complex geometries, containing turbulence, heat transfer, combustion, two-phase flow interactions. [19].

In order to validate the code performance in application to the current problem, LES of fully-developed turbulent plane channel flow was performed using $76 \times 64 \times 64$ grid for the channel size of $2\pi\delta \times 2\delta \times \pi\delta$, where δ is the channel half-width, for Reynolds number $Re_\tau = 180$ based on friction velocity and channel half-width. Grid resolution in wall units is: $\Delta\,x^+ = 14$, $\Delta\,y^+ = 0.4 - 14$, $\Delta\,z^+ = 8.8$. Three eddy viscosity models are tested: Smagorinsky model with van-Driest wall functions, Smagorinsky model without wall functions and dynamic Smagorinsky model with local averaging (global averaging, i.e. averaging along the planes parallel to the wall was not implemented for purpose, since it will not be possible in the riblet case). Computational time step was kept at $\Delta\,tU_l/\delta = 0.05$ for all the three models. Comparison of the mean velocity and turbulent Reynolds stresses, all in wall units, with DNS of Abe et al. [20] is shown in Figures 1a and 1b, respectively. It is seen right away that Smagorinsky model without wall functions shows the worst agreement with DNS results. Smagorinsky model with wall functions performs the best. Superiority of classical Smagorinsky model over dynamic model in this case is explained by the absence of global spanwise averaging in the dynamic model. It is known that dynamic model can produce large local negative values of Smagorinsky coefficient, which are usually smoothed by averaging. Without global averaging these negative values contaminate the results. Therefore, dynamic model might not be a good choice for three-dimensional turbulent flows.
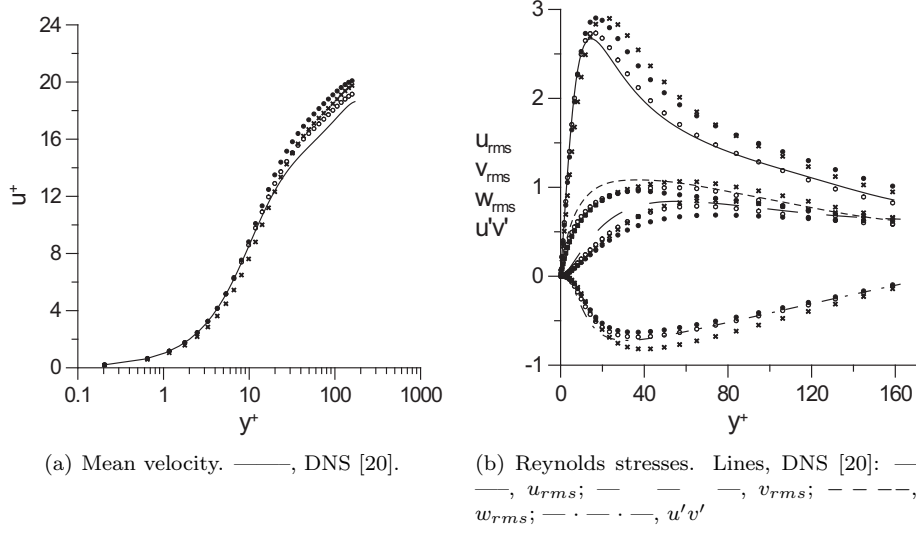
(a) Mean velocity. ———, DNS [20].

(b) Reynolds stresses. Lines, DNS [20]: ———, u_{rms}; — — —, v_{rms}; — — — —, w_{rms}; — · — · —, $u'v'$

Figure 1: Mean velocity and turbulence Reynolds stresses for the plane channel flow. ∘, Smagorinsky model with wall functions; ×, Smagorinsky model without wall functions, •, dynamic model with local averaging.

3 Geometry of the Structured Surfaces

3.1 Conventional and Modified Geometry

As shown in Figure 2, conventional, or two-dimensional structured surfaces or riblets, are the wall grooves aligned in the direction of the freestream flow. The riblet spanwise separation s and the shape of the cross-section are the main adjustable parameters. Previous research efforts identified V-grooves (shown in Figure 2) as an optimum riblet cross-section [5], with an optimum height and spacing of about $15\nu/u_\tau$. It was further confirmed that the riblet configuration continues to remain drag reducing as long as the height and spacing of the grooves do not exceed $25\nu/u_\tau$, after which it becomes drag increasing [6, 8].

The proposed modification is to introduce a spanwise variation into the riblet geometry [17], so that riblets form sinusoidal waves rather than straight lines (see Figure 3) and become three-dimensional, rather than two-dimensional structures. The new shape can be described by the following equation

$$z'(x) = a\,\sin(\frac{2\,\pi}{\lambda}\,x), \tag{1}$$

where $z'(x)$ is the deviation of the spanwise coordinate of the sinusoidal riblet surface from the corresponding coordinate of the straight riblet. Two more parameters are therefore introduced by changing the shape of the riblets, amplitude a and wavelength λ of the sinusoidal shape function. Identifying an
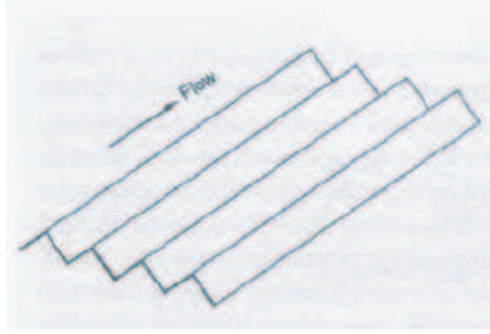
3

Figure 2: Three dimensional view of conventional structured surfaces. Adapted from Ref. [9]

.

(a) Conventional (two-dimensional) structures
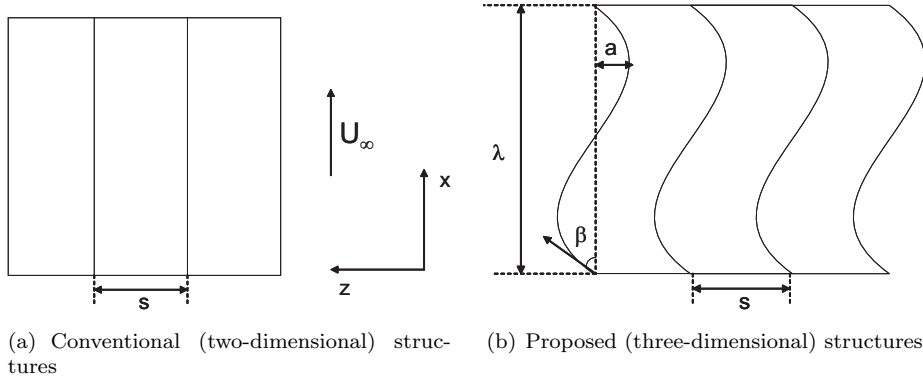

(b) Proposed (three-dimensional) structures

Figure 3: Comparison between two-dimensional and three-dimensional structured surfaces. View from above.

optimum combination of those parameters is an important task for future research.

3.2 Computational Setup

Computational geometry for riblet calculations consists of a channel whose top wall is a flat wall and bottom wall is covered with riblets. Riblets have triangular cross-section with the riblet ridge angle $\alpha = 60°$. The difference between straight two-dimensional riblets and sinusoidal three-dimensional riblets is highlighted in Figure 3. Three-dimensional view of the sinusoidal riblets is available in Figure 4. Parameters of the computational domain are summarized for the three simulated cases in Table 1 in δ units and in Table 2 in wall units. Here δ is half of the distance between the midpoint between tip and valley on a riblet wall and a flat wall and thus corresponds to the half-width of the plane

4

Case	L_x/δ	L_z/δ	s/δ	h/δ	a/δ	λ/δ	$N_x \times N_y \times N_z$
2D	3.22	0.93	0.1164	0.1	0	0	$16 \times 64 \times 128$
3D, case 1	3.22	0.93	0.1164	0.1	0.1	3.22	$16 \times 64 \times 128$
3D, case 2	6	0.93	0.1164	0.1	0.19	6	$32 \times 64 \times 128$

Table 1: Parameters of the computational domain in δ units.

Case	L_x^+	L_z^+	s^+	h^+	a^+	λ^+	$\Delta x^+ \times \Delta y^+ \times \Delta z^+$
2D	580	165	21	18	0	0	$36 \times (0.4 - 14) \times 1.28$
3D, case 1	580	165	21	18	18	580	$36 \times (0.4 - 14) \times 1.28$
3D, case 2	1080	165	21	18	34	1080	$33 \times (0.4 - 14) \times 1.28$

Table 2: Parameters of the computational domain in wall units.

channel with the same cross-sectional area. L_x and L_z are streamwise and spanwise computational periods (as periodic boundary conditions are used in these directions), s is the riblet spacing and h is the riblet height. For the two sinusoidal cases, wavelength λ and amplitude a are varied in a manner so that the maximum slope of the sinusoidal curve $2\pi a/\lambda$ remains constant corresponding to an angle $\beta = 11.3°$ (Figure 3). Size of the computational domain is chosen large enough to guarantee that natural coherence of organized turbulence structures in a boundary layer is not disturbed by insufficient domain size ($L_x^+ > 300, L_z^+ > 100$) [21]. Current computational grid is non-orthogonal, see $y - z$ view of the grid in Figure 5. Reynolds number based on δ and bulk velocity is 2730. This Reynolds number corresponds to $Re_\tau = 180$ based on a friction velocity which would develop in a plane channel flow with the same bulk Reynolds number. Computations are initialized by adding synthetic turbulent fluctuations to the laminar solution. Calculations are advanced with the time step $\Delta t U_b/\delta \sim 0.03$, or $\Delta t^+ \sim 0.3$. No-slip boundary conditions are used at the riblet surface and at the top wall, while periodic boundary conditions are employed in streamwise and spanwise directions. To account for a streamwise pressure gradient in the formulation of periodic boundary conditions, constant forcing term is introduced in a streamwise momentum equation canceling the corresponding pressure gradient term. These calculations are performed with the free turbulence approach, i.e. calculations are initialized by, first, obtaining the laminar solution, and, second, adding synthetic turbulence fluctuations to the laminar solution. After some initial transient time ($tU_b/\delta \sim 900$) synthetic turbulence develops into a natural turbulence inherent to this flow, and statistics is then accumulated for the fully-developed turbulent flow for additional time of $tU_b/\delta \sim 1500$.
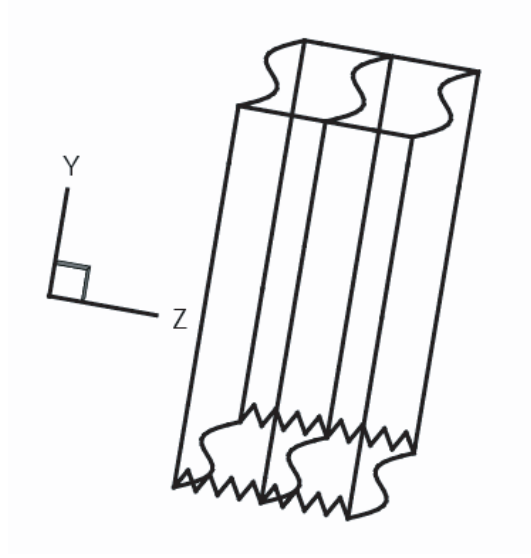
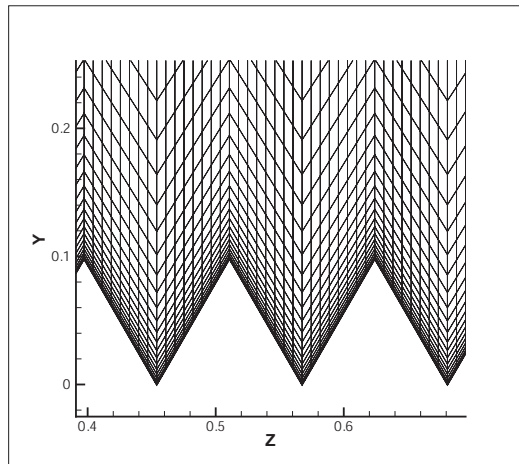Figure 4: Three-dimensional view of the computational domain for the sinusoidal riblet geometry.

Figure 5: $y - z$ view of the numerical grid.

4 Simulations of Two-Dimensional Structured Surfaces

4.1 Results

In this section, results obtained by the LES simulations of turbulent flow over two-dimensional structured surfaces are shown. Three subgrid-scale models are investigated: classical Smagorinsky model [22] with van Driest wall functions [23], modified Smagorinsky model [24] and dynamic Smagorinsky model [25] with local averaging. In a classical Smagorinsky model, eddy viscosity $\nu_{t,\,smag}$ is approximated as

$$\nu_{t,\,smag} = C_{smag}^2 \, \Delta^2 \, (2 \, \overline{S}_{i\,j} \, \overline{S}_{i\,j}), \tag{2}$$

where Δ is the LES-filter width and $\overline{S}_{i\,j} = (\partial \overline{u}_i / \partial x_j + \partial \overline{u}_j / \partial x_i)/2$ is the filtered rate of strain tensor. C_{smag} is the Smagorinsky coefficient which, when van Driest wall functions are used, is defined as

$$C_{smag} = C_{0,\,smag} \, (1 - e^{-y^+/A}), \tag{3}$$

where $C_{0,\,smag}$ is the base constant chosen to be 0.0165 in the present second-order solver to minimize the dissipation, $A = 26$ is the van Driest constant and y^+ is the distance to the wall in wall units.

In a modified Smagorinsky model, eddy viscosity $\nu_{t,\,mod}$ is obtained as

$$\nu_{t,\,mod} = (\nu_{t,\,smag}^2 + \nu^2)^{1/2} - \nu, \tag{4}$$

where $\nu_{t,\,smag}$ is the eddy viscosity of a classical Smagorinsky model defined by equation (2) with C_{smag} defined by equation (3), ν is the laminar viscosity. This modification accounts for the dependence of eddy viscosity on Δ/η, where η is the Kolmogorov scale, missing in a classical Smaroginsky model with constant coefficient [24].

Results are compared with DNS calculations of Choi et al. [6] performed for the same geometry and a similar Reynolds number $Re_b = 2800$. The value of the accumulated time-averaged drag reduction R_D obtained with the three models versus the non-dimensional computational time tU_b/δ is presented in Figure 6. Drag reduction is defined as

$$R_D = \frac{D_f - D_r}{D_f} \times 100\%, \tag{5}$$

where

$$D_f = \mu \int_{A_f} \frac{\partial u}{\partial n} \, d\,A_f,$$
$$D_r = \mu \int_{A_r} \frac{\partial u}{\partial n} \, d\,A_r; \tag{6}$$

D_f, D_r, A_f and A_r are the values of drag and the surface area for the flat and riblet walls, respectively. First, it is seen that quite a long time, tU_b/δ 1000, is
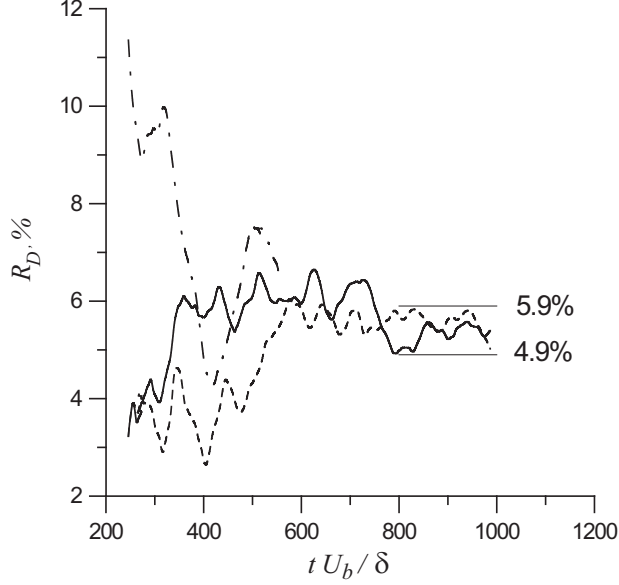
7

Figure 6: Value of the drag reduction versus non-dimensional computational time. ———, classical Smagorinsky model; − − − modified Smagorinsky model; − · − · −, dynamic model with local averaging.

required to reduce the fluctuations in R_D to about $\pm 0.5\%$. Classical Smagorinsky model and modified Smagorinsky model converge to R_D value of about $5.4 \pm 0.5\%$ at tU_b/δ 1000. Dynamic model with local averaging was run for a shorter time, so its computed R_D value of 6.5% would most likely drop down to $\sim 5.4\%$ as well. This value is consistent with the typical drag reduction values for the riblets with triangular cross-section reported in other experimental and computational studies [1, 2, 3, 4, 5, 6, 7, 8]. Drag reduction of 6% was obtained in DNS calculations of Choi et al. [6]. However, their averaging time was only $tU_b/\delta \sim 330$, after which, according to their estimation, the remaining fluctuations of averaged wall-shear rates were about $\pm 2\%$. It is confirmed by the Figure 6 that fluctuations are still quite significant after the averaging time of $tU_b/\delta \sim 330$, indeed about $\pm 2\%$.

Turbulence statistics for the three models is compared in Figure 7, where mean streamwise velocity as well as root-mean square velocity fluctuations are shown. Results from DNS of Choi et al. [6] are also plotted for comparison. Mean velocity is normalized with U_l to be consistent with the plots of Choi et al. [6] (U_l is the centerline velocity which would occur in a laminar plane channel flow with the same bulk velocity, i.e. $U_l = 1.5\,U_b$). Velocity fluctuations are normalized with U_c, where U_c is the turbulent centerline velocity. It can be seen that dynamic model with local averaging significantly underpredicts normal and spanwise Reynolds stresses. Misbehavior of the dynamic model is explained by the absence of averaging along the homogeneous directions as
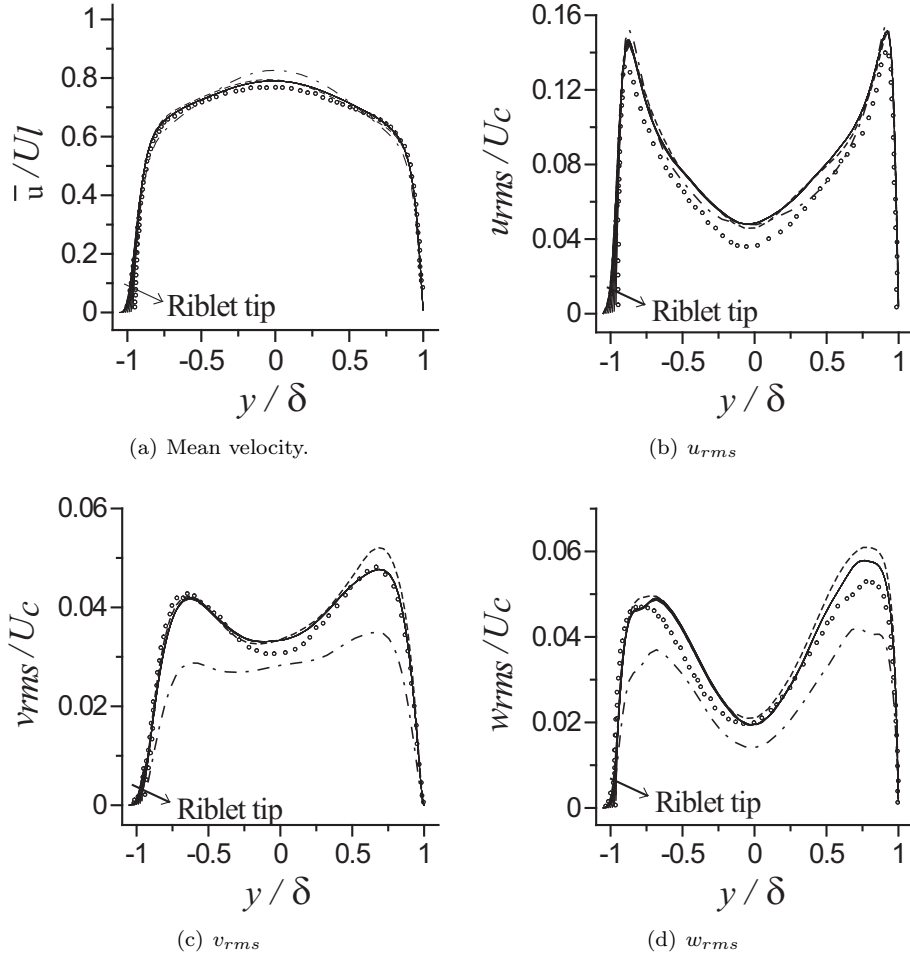
8

(a) Mean velocity.

(b) u_{rms}

(c) v_{rms}

(d) w_{rms}

Figure 7: Turbulence statistics. ———, classical Smagorinsky model; $- - -$ modified Smagorinsky model; $- \cdot - \cdot -$, dynamic model with local averaging, $\circ$, DNS of Choi et al. [6]

usually done for a plane channel. Both classical Smagorinsky and modified Smagorinsky models show generally good agreement with DNS data [6], but modified Smagorinsky model results in slightly higher values of normal and spanwise velocity fluctuations on a flat wall. Since superiority of the modified Smagorinsky model over the classical model was not observed in this case, the authors decided to choose classical Smagorinsky model for the calculations of sinusoidal riblets.

4.2   Drag Reduction Mechanism

Reduction of turbulent fluctuations by riblets demonstrated above signifies a decrease in a turbulent momentum transfer above the riblet surface and, as a consequence, decrease in turbulent shear stresses and, finally, skin-friction drag. However, exact mechanisms explaining why the turbulence is suppressed by the presence of riblets proposed in the open literature can be divided into two groups. One group postulates that riblets impede the cross-flow motion by hampering the fluctuating cross-flow component w'. This leads to the reduction in a turbulent momentum transfer close to the wall, and, finally, decrease in the turbulent shear stress. Robinson [26] hypothesized that riblets impede the cross-stream flow necessary to replace the near wall fluid that is ejected during turbulence production events. Bechert [8] introduced a so-called "protrusion height" which is basically a geometrical property of any specific riblet configuration, and related the protrusion height to the ability of riblets to impede cross-flow. Another group states that interaction of riblets with quasistreamwise vortices is responsible for drag reduction. Quasistreamwise vortices are associated with creation of high skin friction zones in a turbulent boundary layer by bringing high-speed fluid towards the wall during the turbulent sweep events [16, 27]. Hypothesis of Choi [16] is a compromise between the two groups: he thinks that riblets restrain the cross-flow motion of the streamwise vortices, thus reducing the skin-friction. Choi et. al. [6] propose a mechanism, by which streamwise vortices are displaced by riblets further from the wall. They explain the decrease of performance for the riblets with $s^+ > 25$ by the ability of streamwise vortices to fit between the larger spaced riblet tips. Their theory is based on assumption that the typical diameter of the streamwise vortices is $d^+ \sim 30$. Pollard [28] agrees that riblets effectively displace the turbulence production events (sweeps and ejections) away from the wall, resulting in the reduced wall shear stress.

Current results support the second mechanism by showing that quasistreamwise vortices are indeed displaced away from the riblet surface compared to the flat wall (see Figure 8 showing the spanwise view of instantaneous streamwise vorticity). Three-dimensional view of coherent vortical structures identified by Q-criterion and displayed in Figure 9 once again confirms the reduction of turbulent activity next to the riblet surface. Displacement of streamwise vortices further from the riblet surface, suppression of their spanwise meandering and overall reduction in the amount of vortices are evident.
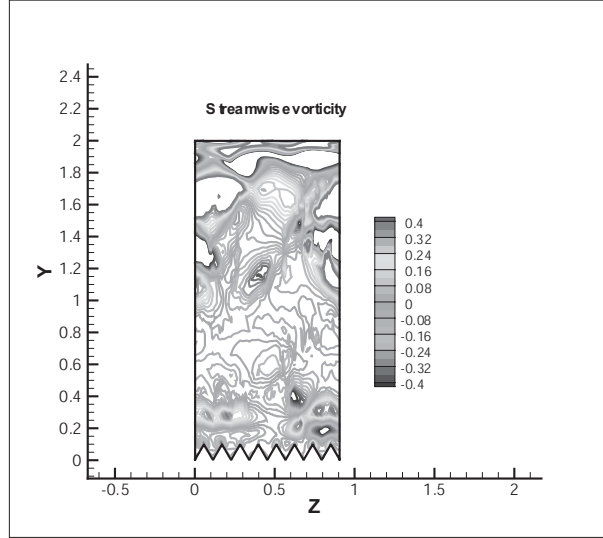
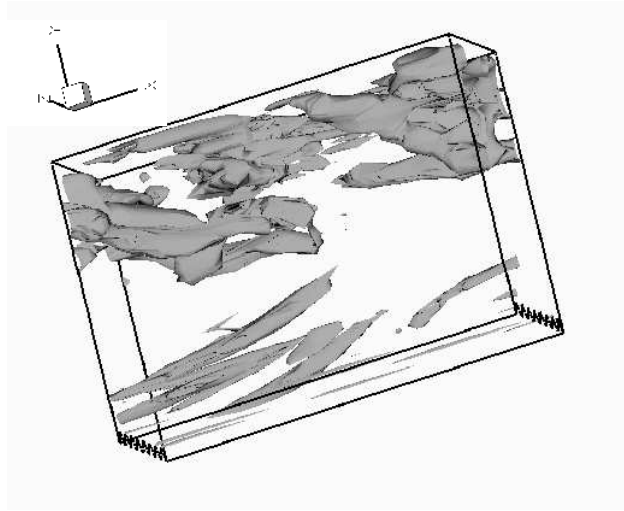Figure 8: Spanwise view of instantaneous streamwise vorticity.

Figure 9: Coherent vortical structures identified by Q-criterion.

11

5 Simulations of Three-Dimensional Structured Surfaces

5.1 Laminar Flow

Since three-dimensional structured surfaces is a relatively new development, before performing turbulent calculations of this geometry, we present detailed analysis of the laminar flow for the case 1 simulations (see Tables 1 and 2). Laminar flow calculations were carried out for the same Reynolds number $Re = 2730$ based on the bulk velocity, or $Re = 4095$ based on the centerline velocity. Longitudinal view of spanwise velocity developed over the sinusoidal riblet surface and normalized with the streamwise centerline velocity, w/U_l, is shown in Figure 10 for ($x - y$ cross-section taken through the riblet valley is plotted). An oscillatory motion of the mean flow is evident, signified by the change of the sign of spanwise velocity w in the riblet surface boundary layer from negative to positive and back to negative with the streamwise distance. If we plot spanwise velocity profiles $w(x)$ for several distances from the wall y/δ (Figure 11a), we can notice that spanwise velocity distributions in the riblet surface boundary layer follow the shape of the sinusoidal slope dz'/dx. This is natural, since spanwise velocity induced by the rotation of the mean velocity vector due to the wavy motion is proportional to the slope.

By analogy with the flow near an oscillating wall, a crossflow boundary layer is developed, which confines three-dimensional effects to the layer of some finite thickness. In order to predict crossflow layer thickness and maximum spanwise velocity for any given riblet configuration, a theoretical approach based on an analogy with the Stokes layer is proposed. Stokes layer is an analytical solution of the Navier-Stokes equations for the case when a flat plate oscillates tangentially in a still fluid described by Schlichting [29]. Although it is a different phenomenon, an analogy can be followed if one takes a lagrangian approach and moves with the fluid particle in a crossflow boundary layer, which indeed follow and oscillatory trajectory. To make a comparison with the Schlichting solution, one can write an oscillation period as $T = \lambda/u^\star$, where $u^\star$ is some characteristic velocity of streamwise motion in a crossflow boundary layer. We approximate $u^\star$ as the streamwise velocity of the plane laminar channel flow at y location where the Stokes layer vorticity is maximum, i.e. at the distance of $y^\star \sim \delta_s/4$ (see [14, 29]), where

$$\delta_s = \pi \sqrt{2\,\nu/\omega} \tag{7}$$

is the Stokes layer thickness (defined here as one half of the "penetration depth" in [29]), $\omega = 2\,\pi/T$.

Taking into account that the Stokes layer thickness is small compared to the channel half-width for the considered Reynolds number, one can approximate $u^\star$ using a linear relationship derived from the analytical solution for the plane Poiseuille flow valid for small distances from the wall: $u^\star/U_l \sim 2\,y^\star/\delta = \delta_s/2\,\delta$, where U_l is the laminar centerline velocity and δ is the channel half-width.

12

Therefore, expanding definition of $\omega = 2\,\pi/T = 2\,\pi\,u^\star/\lambda$ as

$$\omega = \frac{\pi\,U_l\,\delta_s}{\lambda\,\delta} \tag{8}$$

and substituting equation (7) for the Stokes layer thickness δ_s, one can solve for ω:

$$\omega = \sqrt[3]{\pi^4\,2\,\nu\left(\frac{U_l}{\lambda\,\delta}\right)^2} \tag{9}$$

This formula can be expected to hold only for small amplitudes a/λ of the sinusoidal riblet shape, since $u^\star$ is estimated assuming that the spanwise crossflow motion does not influence the mean streamwise velocity. For large amplitudes, spanwise oscillatory motion will most likely affect the streamwise velocity in the crossflow boundary layer, resulting in smaller effective velocity $u^\star$ and smaller oscillation frequency than the one predicted by equation (9). For the current simulation parameters, the value of non-dimensional frequency $\omega\,\delta/U_l = 0.17$ is obtained, which allows to estimate the crossflow boundary layer thickness $\delta_s/\delta = 0.16$ from equation (7), which is the correct estimate according to the Figure 10. According to Shclichting [29], spanwise velocity in a Stokes layer scales with the "wall speed" w_0, or maximum amplitude of the wall velocity. In a riblet crossflow boundary layer, similar parameter would be the spanwise velocity induced by the rotation of a characteristic velocity $u^\star$ to an angle corresponding to the local slope (dz'/dx). For small amplitudes a/λ, this can be approximated as

$$w_0\,(x) = u^\star(dz'/dx) = a\,\omega\,cos(\frac{2\,\pi\,x}{\lambda}) \tag{10}$$

(refer to equation (1)).

Note that the Stokes layer in a wall-oscillating case and a riblet crossflow boundary layer developed in the current case, in spite of their analogy, are different in nature. Stokes layer is time-dependent, whereas current crossflow layer is stationary. Also, spanwise wall velocity is oscillating in the Stokes layer, whereas it is always zero in the current case due to the no-slip conditions. Therefore, if we want to compare spanwise velocity distribution with that of a Stokes layer, we should only consider the Stokes layer profiles corresponding to the zero wall velocity, i.e. oscillation phases $\omega\,t = \pi/2$ or $\omega\,t = 3\,\pi/2$. Comparison of the spanwise velocity profiles $w/w_0(\eta)$, where $\eta = y\,\sqrt{\omega/(2\,\nu)}$ is the similarity variable, with the Stokes layer solution taken at $\omega\,t = \pi/2$, when the wall velocity is zero, is plotted in Figure 11b. For comparison, we chose four different streamwise locations along the computational domain corresponding to $x/\lambda = 0$, 0.13, 0.5 and 0.64. Note that w_0 calculated with equation (10) can achieve both positive and negative values, which explains why all the scaled profiles fall on a single curve for both positive and negative spanwise velocities in a crossflow layer (cf. Figure 10). Although these are not the same phenomena, the similarity of the corresponding spanwise velocity profiles is striking, signifying that the viscous mechanisms responsible for the creation of boundary
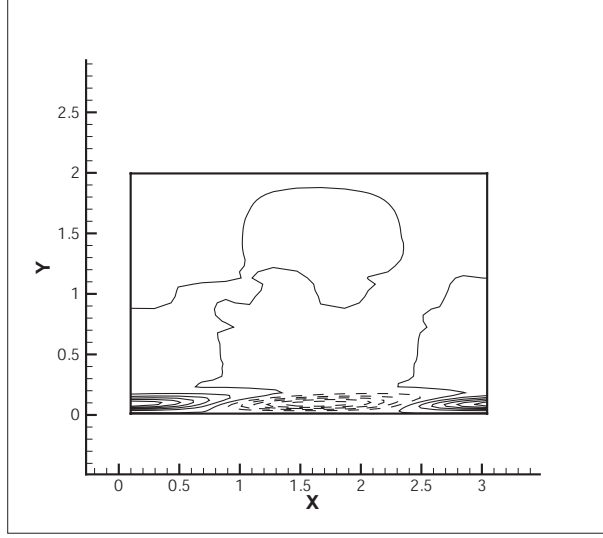
Figure 10: Longitudinal view of spanwise laminar velocity, w/U_l. Solid lines – positive values, dashed lines - negative. Velocity range: -0.005 to 0.005, contour increment: 0.001.

layers in these two cases are the same. It also shows that the crossflow boundary layer thickness δ_s and the amplitude of spanwise velocity oscillations $w_0(x)$ are estimated correctly by the current theoretical approach. It is worth noting that the maximum spanwise velocity w_{max} achieved in the current simulations can be predicted as $w_{max} = 0.3\,w_{0\,max} = 0.3\,a\omega$ (see also equation (10)). This leads to $w_{max} = 0.0051\,U_l$, which corresponds exactly to the maximum values observed in the simulations, see Figure 10. This analysis shows that, first, a similarity between the riblet crossflow layer and a Stokes layer is established, and, second, that the current theory allows to construct correct relationship between the wavelength of the riblet shape λ and the period of the wall oscillation T in a laminar case.

5.2 Turbulent Flow

In order to check whether this similarity of a riblet crossflow boundary layer with a Stokes layer over a spanwise-oscillating plate will further result in similar drag reduction benefits, values of R_D defined in Equation (5) are plotted versus non-dimensional computational time in Figure 12 for cases 1 and 2 of three-dimensional structures (see Tables 1 and 2) compared to two-dimensional structures. It is seen that drag reduction is reduced to a negative value for the Sinus 1 case, where the wavelength of the oscillations is chosen to be $\lambda/\delta = 3.22$. Probably, such a short oscillation length introduces some kind of unsteadiness into the near-wall turbulence and beneficial properties of riblets are completely subdued by these unfavorable effects. It is not unexpected, since drag reduction

(a) Streamwise profile, $w(x)$, for several distances from the wall, y/δ. Slope of the riblet surface, dz'/dx, is also shown.

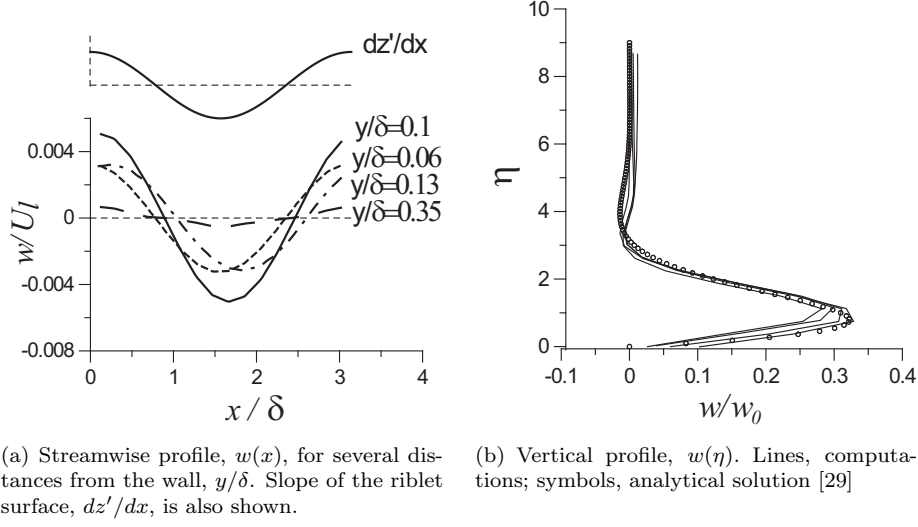(b) Vertical profile, $w(\eta)$. Lines, computations; symbols, analytical solution [29]

Figure 11: Laminar spanwise velocity profiles over the sinusoidal riblet surface.

with the spanwise wall oscillation also strongly depends on the period of the wall oscillations and negative drag reduction values are observed when the period is too short, $T^+ < 25$ [10]. Unfortunately, no explanation of this trend is currently offered. When the oscillation wavelength is almost doubled to $\lambda/\delta = 6$, the drag reduction value rises to $7.4 \pm 0.5\%$, which is almost 50% larger than the drag reduction observed with the straight riblets. It is an author's belief that with the careful choice of riblet oscillation parameters it is possible to raise this value even higher.

The reason for such a dramatic difference in drag reduction properties with the wavelength of riblet oscillations remains unknown and is the subject of the current investigation. Unfortunately, no conclusions concerning the drag reduction mechanism with sinusoidal riblets can be drawn from the turbulence statistics, since all three cases show similar trends (see comparison of turbulence statistics for the two cases of 3D structures with 2D structures in Figure 13). Perhaps, mostly the near-wall flow is affected by the spanwise riblet oscillations and turbulence statistics in the rest of the channel does not change much. Detailed investigation of the near-wall flow and change in behavior of streamwise vortices with the spanwise riblet oscillations is a next step and will hopefully shed some light on the drag reduction mechanism.

6 Conclusions

We show that introducing spanwise sinusoidal variation to the riblet shape can be an effective drag reduction method showing benefits compared to the conventional straight riblets with the correct choice of geometrical parameters. Large
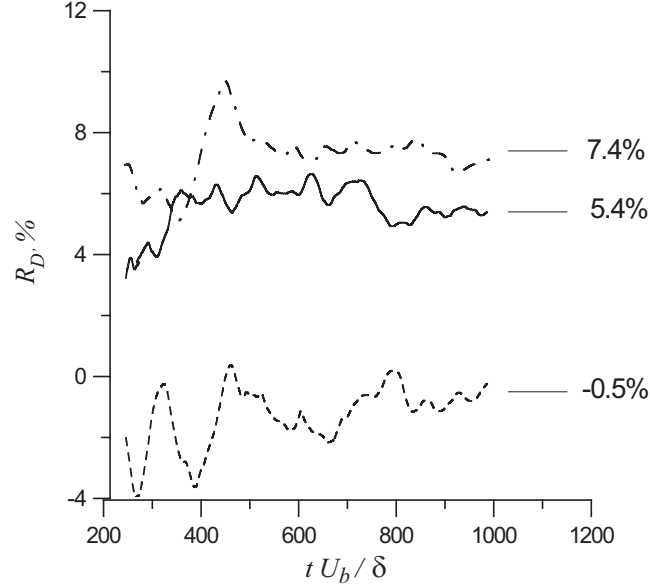
Figure 12: Value of the drag reduction versus non-dimensional computational time. ———, 2D structures; $---$, 3D structures, case 1; $-\cdot-\cdot-$, 3D structures, case 2.

Eddy Simulations are performed for the straight riblets and two sinusoidal riblets with different oscillation wavelengthes. Several turbulence models are considered for the straight riblet case and results are compared to DNS data [6] for the same configuration. Classical Smagorinsky model provides the best results for this case and is used for sinusoidal riblet calculations. For sinusoidal riblets, drag reduction depends strongly on the wavelength of the sinusoidal oscillations. For a smaller wavelength, $\lambda/\delta = 3.22$, no drag reduction is observed. For a larger value, $\lambda/\delta = 6$, drag reduction of 7.4% is achieved compared to 5.4% in a straight case. This signifies almost 50% of the drag reduction increase and it is believed that even higher benefits can be obtained by careful optimization of spanwise riblet variation parameters. Mechanism explaining drag reduction with sinusoidal riblets is currently under investigation. Preliminary conclusion is that the effects are confined to the near-wall layer, since turbulence statistics in the rest of the channel does not seem to be affected by the spanwise riblet oscillations.

Acknowledgements

(a) Mean velocity.

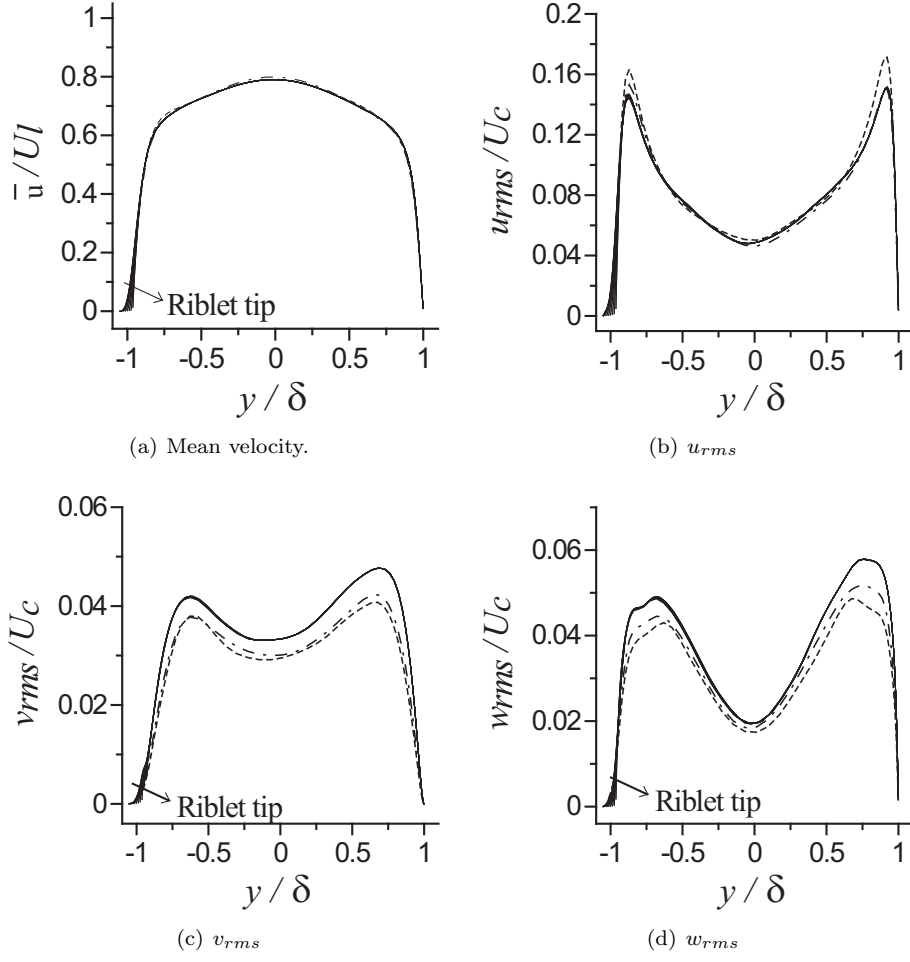(b) u_{rms}

(c) v_{rms}

(d) w_{rms}

Figure 13: Turbulence statistics. ———, 2D structures; − − −, 3D structures, case 1; − · − · −, 3D structures, case 2.

References

[1] M. J. Walsh. Drag characteristics of v-groove and transverse curvature riblets. In *Viscous Flow Drag Reduction*, ed. G. R. Hough, pages 168–184. AIAA, New York, 1980.

[2] M. J. Walsh. Turbulent boundary layer drag reduction using riblets. AIAA Paper 82–0169, 1982. New York.

[3] M. J. Walsh. Riblets as a viscous drag reduction technique. *AIAA J.*, 21:485–486, 1983.

[4] M. J. Walsh and A. M. Lindemann. Optimization and application of riblets for turbulent drag reduction. AIAA Paper 84–0347, 1984. New York.

[5] M. J. Walsh. Riblets. In *Viscous Drag Reduction in Boundary Layers*, eds. D. M. Bushnell and J. N. Heffner, pages 203–261. AIAA, Washington, D.C., 1990.

[6] H. Choi, P. Moin, and J. Kim. Direct numerical simulation of turbulent flow over riblets. *J. Fluid Mech.*, 255:503–539, 1993.

[7] D. Goldstein, R. Handler, and L. Sirovich. Direct numerical simulation of turbulent flow over modelled riblet covered surface. *J. Fluid Mech.*, 302:333–376, 1995.

[8] D. W. Bechert, M. Bruse, W. Hage, J. G. T. Van Der Hoeven, and G. Hoppe. Experiments on drag-reducing surfaces and their optimization with an adjustable geometry. *J. Fluid Mech.*, 338:59–87, 1997.

[9] M. Gad-El-Hak. *Flow Control*. Cambridge University Press, 2000.

[10] W. J. Jung, N. Mangiavacchi, and R. Akhavan. Suppression of turbulence in wall bounded flows by high-frequency spanwise oscillations. *Phys. Fluids*, 8:1605–1607, 1992.

[11] F. Laadhari, L. Skandaji, and R. Morel. Turbulence reduction in a boundary layer by a local spanwise oscillating surface. *Phys. Fluids*, (10):3218–3220, 1994.

[12] K.-S. Choi and M. Graham. Drag reduction of turbulent pipe flows by circular-wall oscillation. *Phys. Fluids*, 10(1):7–9, 1998.

[13] K.-S. Choi, J. R. DeBisschop, and B. R. Clayton. Turbulent boundary-layer control by means of spanwise-wall oscillation. *AIAA J.*, 36:1157, 1998.

[14] K.-S. Choi and B. R. Clayton. The mechanism of turbulent drag reduction with wall oscillation. *Int. J. Heat and Fluid Flow*, 22:1–9, 2001.

[15] K.-S. Choi. Near-wall structure of turbulent boundary layer with spanwise-wall oscillation. *Phys. Fluids*, 14(7):2530–2542, 2002.

[16] K.-S. Choi. Near-wall structure of a turbulent boundary layer with riblets. *J. Fluid Mech.*, 208:417–458, 1989.

[17] Y. Charron and E. Lepesan. Surface structurée tri dimensionnelle à onde transverse en vue d'une réduction de la traînée aérodynamique. Patent FR 2899 945, October 2007.

[18] A. Baron and M. Quadrio. Turbulent boundary layer over riblets: Conditional analysis of ejection-like events. *Int. J. Heat and Fluid Flow*, 18:188–196, 1997.

[19] F. Archambeau, N. Méchitoua, and M. Sakiz. Code_saturne: a finite volume code for the computation of turbulent incompressible flows - industrial applications. *Int. J. Fin. Vol.*, 1, 2004.

[20] H. Abe, H. Kawamura, and Y. Matsu. Direct numerical simulation of a fully developed turbulent channel flow with respect to reynolds number dependence. *ASME Journal of Fluids Engineering*, 123:382, 2001.

[21] J. Jiménez and P. Moin. The minimal flow unit in near-wall turbulence. *J. Fluid Mech.*, 225:213–240, 1991.

[22] J. Smagorinsky. General circulation experiments with the primitive equations. *Journal of Monthly Weather Review*, 91(3):99–164, 1963.

[23] E. R. Van Driest. Turbulent boundary layer in compressible fluids. *J. Aerospace Sci.*, 18(3):145–160, 1951.

[24] J. Meyers and P. Sagaut. On the model coefficient for the standard and the variational multi-scale smagorinsky model. *J. Fluid Mech.*, 569:287–319, 2006.

[25] M. Germano, U. Piomelli, P. Moin, and W. H. Cabot. A dynamic subgrid-scale eddy viscosity model. *Physics of Fluids, A3*, pages 1760–1765, 1991.

[26] S. K. Robinson. Coherent motions in the turbulent boundary layer. *Ann. Rev. Fluid Mech.*, 23:601, 1991.

[27] H. Choi, P. Moin, and J. Kim. Turbulent drag recution: Studies of feedback control and flow over riblets. TF-55 83-0230, 1992. Department of Mechanical Engineering. Stanford University, Stanford, California.

[28] A. Pollard. Passive and active control of near-wall turbulence. *Prog. Aerospace Sci.*, 33:689–708, 1997.

[29] H. Schlichting. *Boundary-layer theory.* Berlin; New York: Springer, 8 rev. and enl. edition, 2000.